Reactive Molecular Dynamics of Hypervelocity Collisions of PETN Molecules

A. C. Landerville,*,† I. I. Oleynik,† and C. T. White‡

Department of Physics, University of South Florida, Tampa, Florida 33620, and Chemistry Division, Naval Research Laboratory, Washington, D.C. 20375

Received: June 25, 2009; Revised Manuscript Received: August 31, 2009

Born−Oppenheimer direct dynamics classical trajectory simulations of bimolecular collisions of PETN molecules have been performed to investigate the fundamental mechanisms of hypervelocity chemistry relevant to initiating reactions immediately behind the shock wavefront in energetic molecular crystals. The solid-state environment specifies the initial orientations of colliding molecules. The threshold velocities for initiating chemistry for a variety of crystallographic orientations were correlated with available experimental data on anisotropic shock sensitivity of PETN. Collisions normal to the planes (001) and (110) were found to be most sensitive with threshold velocities on the order of characteristic particle velocities in detonating PETN. The production of NO_2 is the dominant reaction pathway in most of the reactive cases. The simulations show that the reactive chemistry, driven by dynamics rather than temperature during hypervelocity collisions, can occur at a very short time scale (10^{-13} s) under highly nonequilibrium conditions.

I. Introduction

In spite of over a century of intensive experimental and theoretical investigations, an understanding of the mechanisms of detonation in explosives [or energetic materials (EMs)], including the shock-induced chemical reactions, still remains one of the challenging problems of chemical physics.[1−5] The classic continuum theories of detonation were successful in predicting macroscopic properties, such as detonation speed and detonation pressure, using mostly hydrodynamic and thermodynamic descriptions with very little detailed input involving the chemistry of energetic materials.[5−7] In particular, Chapman and Jouguet (C−J) assumed that the speed of detonation does not depend on the rate of the chemical reactions because they proceed so fast that the chemical transformation from reactants to detonation products occurs within the infinitesimally thin layer at the shock wavefront.[8,9] The C−J model of detonation was later replaced by the Zeldovich, von Neumann, and Doering (ZND) model[10−12] which introduced a finite reaction rate and associated finite reaction zone. Despite these advancements in detonation theory, the detailed mechanisms of the chemical reaction dynamics were unnecessary.

As experimental studies progressed toward exploring ever smaller time and length scales, a detailed knowledge of the atomic-scale mechanisms of detonation became increasingly important for explaining the observed phenomena.[13] The more important questions include how detonation is initiated and sustained and what mechanisms are responsible for shock-induced chemical reactions, including both the first endothermic steps and the following exothermic reactions toward detonation products. One way to include chemistry is to assume that there is a local thermal equilibrium characterized by a local temperature, and to use standard transition state theory (TST) to describe the reaction rates. Unfortunately, while such an approach has been highly successful for thermal decomposition studies,[14−17] it ultimately ignores the highly nonequilibrium initial processes of the shock-wave mechanical energy transfer to the individual molecules when the notions of thermal equilibrium and temperature are ill-defined immediately behind the shock wavefront.

This problem attracted the attention of Henry Eyring, one of the founders of chemical reaction dynamics and transition state theory.[18] In an attempt to explain the experimentally observed slow increase of the reaction rates with the shock temperature compared to that predicted by TST, he proposed a concept of *starvation kinetics*.[19] The conventional view of endothermic bond breaking involves the concentration of a sufficient amount of energy along the reaction coordinate which is coupled with a thermal bath of surrounding molecular modes. This process is substantially less efficient when the reaction coordinate must draw its energy from a thermal bath that is in nonequilibrium with the translational degrees of freedom of the reacting molecule; e.g., molecular collisions cause deformations which lead to one part of the reacting molecule being in nonequilibrium with another part. This reduces the probability of concentration of the activation energy within the modes along the reaction coordinate.[19]

A further development of the theory of shock-induced chemical reactivity was the multiphonon up-pumping model.[20−24] Assuming the standard notion of TST, i.e., the activation of a reactive vibrational normal mode, focus was placed on the mechanism of energy transfer from the shock wave to the high-frequency vibration modes of the molecules. According to this theory, the shock wave produces a bath of excited phonons of the molecular crystal which excite the low frequency doorway vibration modes (e.g., modes involving the entire molecule) due to anharmonic phonon−doorway mode coupling. This is followed by energy transfer into the high frequency modes (e.g., stretching modes) via multiphonon up-pumping and intramolecular vibration energy redistribution. Once the up-pumping is complete, within several tens of picoseconds, Arrhenius kinetics becomes valid. Both mechanisms of starvation kinetics and multiphonon up-pumping were incorporated in the non-equilibrium ZND theory of detonation developed by Tarver.[25]

Because of difficulties in real-time experimental investigations of shock-induced chemistry at the onset and during detonation,

† University of South Florida.
‡ Naval Research Laboratory.

10.1021/jp905969y CCC: $40.75
Published on Web 10/09/2009

experimental study of chemical reactivity in energetic materials has been limited to thermal decompositions of EMs at slow heating rates (cookoff).[26−29] Although such studies are important for the evaluation of the thermal stability of explosives, it is not clear whether they are relevant for understanding the fast chemical processes of shock initiation, and the self-sustained propagation of detonation. Only recently, advances in experimental techniques have allowed direct investigation of the chemical reactivity behind the detonation front.[13] For example, shock-induced decomposition chemistry of pentaerythritol tetranitrate (PETN), the EM to be discussed in this paper, was studied using optical transitions and light emission associated with PETN decomposition at the early stages of initiation.[30]

With tremendous advances in computational capabilities, it has become possible to perform computational experiments to study the reactive molecular dynamics at conditions similar to a detonation. One of the major challenges for theory/modeling is the disparate time and length scales associated with the various processes of detonation. For example, the initial shock compression takes place over picoseconds at the nanometer length scale,[31] but the entire reaction zone width is at least several micrometers, while the corresponding time scale to complete chemical reactions is in excess of nanoseconds.

Previous modeling efforts were mostly concentrated on studying the gas-phase thermal decomposition of EMs such as RDX[32] and HMX[33] using transition state theory and density functional theory (DFT) based potential energy surfaces (PES). Classical trajectory simulations using model PES were also performed.[34,35] Several studies of the condensed phase decomposition of EMs were concerned with the rapid heating from normal pressures and temperatures to the C−J point using DFT-based reactive molecular dynamics.[36−39] Using continuum theory constraints introduced into reactive MD simulations, a quasi-metallic state was discovered in shocked nitromethane at detonation conditions.[38] This observation is closely related to another proposal for the initiation of chemistry via electronic excitations of EMs; band gap lowering and excitations around crystal defects under high temperatures and pressures were considered as possible mechanisms of initiation.[40−42]

One promising approach to extend time and length scales of atomic-scale simulations of detonation chemistry is to develop reactive potentials that are capable of describing the fundamental chemistry of bond breaking and remaking.[43−45] By devising reactive-empirical-bond-order (REBO) potentials for modeling a generic AB system, the first molecular dynamics simulations of a self-sustained detonation were performed[45−47] with this model, leading to results consistent with a classic ZND detonation.[46] Very recently, reactive force fields (ReaxFF) have been developed for organic energetic materials[48] which enabled large-scale simulations of reactive shock wave propagation in EMs such as RDX[49−51] and PETN.[52] These simulations provided valuable insight into the reactive chemistry of EMs. However, extreme care should be exercised in making conclusions about the fundamental mechanisms of the detonation chemistry. This is because ReaxFF, although sophisticated, still provides a classical description of the intrinsically quantum mechanical processes of bond breaking and remaking via a complicated functional form and fitting ("or training") of numerous ReaxFF parameters. We believe that, by understanding the mechanisms of chemistry in hypervelocity collisions of EM molecules, further refinement can be made to ReaxFF potentials which may ultimately lead to more accurate modeling of larger detonating systems.

The goal of this work is to investigate the first chemical events in detonating PETN initiated by the propagation of a strong shock wave. In contrast to the models of initiation of chemistry discussed above, which assume some sort of thermal equilibrium within specific groups of molecular degrees of freedom, as well as the existence of a corresponding temperature, special focus is placed on the highly nonequilibrium mechano-chemical regime of direct bond breaking due to hypervelocity molecular collisions initiated by the very fast uniaxial shock compression of a molecular crystal. Such a mechanism was first proposed in the works of Anatoly Dremin[53] and Frank Walker.[54,55] They both suggested that the kinetic energy of the shock wave is initially adsorbed by the translational molecular degrees of freedom which results in the direct endothermic breaking of the intramolecular chemical bonds. Because of the lack of equilibrium, the initiation of chemical reactions in the shock front is not a thermal process; i.e., it is not controlled by temperature which is ill-defined under such nonequilibrium conditions.

The computational studies reported in this paper were performed using quantum-mechanical descriptions of the interatomic interactions described by first-principles DFT. The object of these investigations, PETN, was chosen because of its known dependence of shock-induced initiation of detonation on the crystallographic direction of the shock propagation, as was discovered by Jerry Dick in his classic experiments.[56−59] This property of anisotropic shock response implies a relationship between the high sensitivity of chemical reactivity to the initial mutual orientations of the colliding molecules specified by their relative geometry within the initial crystalline environment.

Although similar hypervelocity collision simulations have been attempted in the past,[60−63] they were performed within a limited subset of initial conditions (fewer directions and velocities sampled) and mostly using the semiempirical electronic structure method PM3,[64,65] which is known to give large errors in predicting heats of reaction and activation energies of organic molecules.[61,66] Our goal is to use first-principles DFT to predict the dynamics of chemical transformation, including the reaction pathways and the associated time scales, as a function of the magnitude of the collision velocity and the initial mutual orientations of two colliding molecules specified by a given direction corresponding to the normal of the associated compression of planes within the molecular crystal. Special attention is paid to identifying the differences between the commonly used thermally activated reaction dynamics and the hypervelocity chemistry initiated by the fast uniaxial compression of the crystal behind the shock wavefront.

It is important to note that, while we assume molecular collisions to be the precursor to the initiation of chemical reactions at the detonation front, we have not simulated collisions involving more than two molecules due to computational expense. Such a study[63] was performed by Decker et al. for nitromethane. They found that, while C−N bond scission was the main reaction pathway in both bimolecular and multimolecular collisions, only one of the higher energy multimolecular collision cases involved the transfer of a hydrogen atom from one molecule to another, a reaction which was not seen in any of the bimolecular cases. However, in general, multimolecular collisions imposed more steric constraint on the colliding molecules which resulted in a higher instance of C−N bond reformation; i.e., threshold velocities became higher than those for bimolecular collisions.[63] Still, in both bimolecular and multimolecular collisions of nitromethane simulated by Decker et al., essentially the same reaction pathway (C−N bond scission) was predominantly observed. Therefore,

while threshold velocities might change by adding more molecules to our collision simulations, we would likely see little difference in the overall chemical dynamics of the hypervelocity collisions, as well as the relative sensitivities of the reactions along different crystallographic directions.

II. Computational Details

The simulation of chemical reactions in the condensed phase is a challenging problem because it requires an accurate quantum mechanical description of interatomic interactions in a system consisting of a very large number of atoms. Because such simulations are currently unfeasible, we devised a simplified model system that contains a manageable number of atoms that are treated quantum-mechanically using first-principles density functional theory under the Born−Oppenheimer approximation, while preserving essential features of the chemistry induced by hypervelocity molecular collisions. Because the major focus is on chemical dynamics initiated by the shock wave, we assume that the initial steps involve the rapid approach and collisions of molecules within adjacent plains normal to the direction of shock compression. Therefore, molecular pairs were extracted from the EM crystal by preserving the local crystalline environment (relative position and orientation). Then, the bimolecular collisions are simulated by assigning the pair of selected molecules the relative velocity and following their collision dynamics.

Reactive MD of bimolecular collisions was studied by integrating the classical Newtonian equations of motion for each atom:

$$M_i \frac{d^2 R_i}{dt^2} = -\frac{\partial V(\{R_i\})}{\partial R_i} \quad (1)$$

where the potential energy $V(\{R_i\})$ and the forces $-\partial V(\{R_i\})/\partial R_i$ are evaluated on-the-fly by solving the Kohn−Sham DFT equations at each time step at fixed nuclear coordinates R_i to obtain the total electronic energy $E_{el}^{DFT}(\{R_i\})$, which serves as a potential energy for nuclear dynamics: $V(\{R_i\}) = E_{el}^{DFT}(\{R_i\})$. Equation 1, together with the initial conditions (discussed below), completely specifies the dynamics of the bimolecular collisions.

The first-principles DFT calculations were performed using the linear combination of atomic orbitals (LCAO) code SIESTA.[68] The effect of the core electrons is taken into account by employing norm-conserving pseudopotentials. The Perdew−Burke−Ernzerhof (PBE) generalized gradient approximation (GGA) density functional is used.[69] The valence electronic states are expanded using the double-ζ plus polarization (DZP) basis set that we specifically optimized to achieve the highest level of accuracy in the description of the energies and forces as compared to the fully converged plane-wave calculations for several configurations of the colliding PETN molecules. A real space energy cutoff of 200 Ry was chosen to give reasonable accuracy without excessive computational expense.

The initial conditions for the reactive collision dynamics simulations were set up by constructing the two-molecule collision complex and specifying initial velocities for each atom of the complex. We are specifically interested in relating the bimolecular reactivity with observed orientation-dependent initiation pressures.[56−59] Therefore, we investigated collisions caused by the compression of crystallographic planes, and consider all possible collisions along directions corresponding to the normals of the following crystallographic planes within the PETN unit cell: (001), (010), (011), (100), (101), (110), and (111). To simplify this selection procedure, each molecule in the crystal lattice was represented with a sphere of radius R which is half the diameter of the molecule. Figure 1 shows this simplified model of the body centered tetragonal PETN crystal with each molecule indexed for the purpose of identifying a specific collision pair used in the simulations.

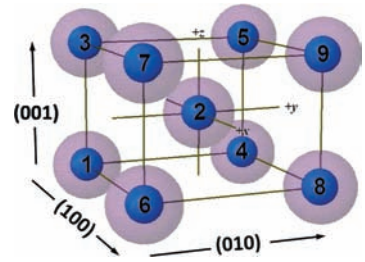

Figure 1. Simplified depiction of the body centered tetragonal PETN lattice using spheres in place of molecules. The numbers on the spheres serve as an index used to identify molecules participating in each collision case. Blue represents zones of head-on collisions, while gray represents zones of glancing collisions.

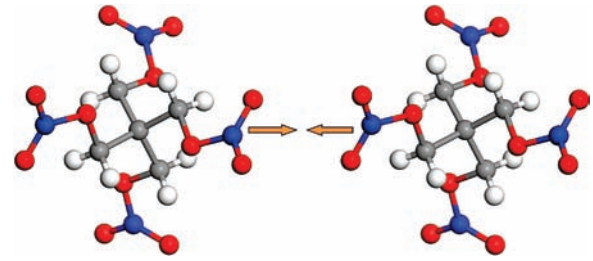

Figure 2. Collision geometry of two PETN molecules set to collide along a specific crystallographic direction.

The inner spheres have a radius of $R/2$, and were used to define two different types of collisions—head-on and glancing. If the inner spheres of two molecules collide upon translation in a particular direction, then the collision is classified as head-on; if only the outer spheres collide, then the collision is labeled as glancing.

Once all possible collisions were found, the associated molecules were isolated in their crystallographic orientation with respect to one another and centered within an empty box. The molecules were then thermally equilibrated to 300 K. Next, one-half the desired collision velocity was applied to each molecule such that they collided in the center of the box, as depicted in Figure 2.

Collision velocities ranging from 3 to 7 km/s were sampled for 13 different orientations. Owing to the computational expense of DFT calculations, a statistical sampling was not performed. However, the statistics is indirectly sampled by running simulations with multiple collision orientations.

The trajectory data obtained from each simulation were analyzed to determine the onset of reaction, the reaction time scale, and the type of products. The lowest velocity at which reactions occurred for any particular direction and orientation was taken to be the threshold velocity for initiating chemistry for that particular case. All of the reactive cases at the threshold velocities share one important feature: the reaction products originate from one molecule, while its colliding counterpart remains chemically intact.[70−72] At higher collision velocities, products were observed to be originating from both molecules. The investigation of the threshold velocities as a function of initial crystalline orientation allows us to make an important conclusion: the reactive initiation dynamics is orientation-

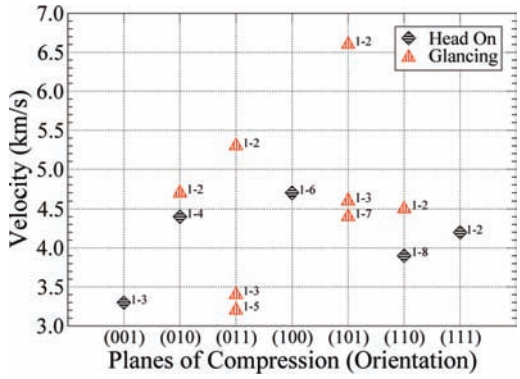

Figure 3. Threshold velocities for initiating chemical reactions for different directions corresponding to the plains of compression shown. The numbers to the right of each point specify the participating molecules in the specific collision case; see Figure 1.

dependent. Indeed, we find that each collision orientation has a different threshold velocity for initiating chemistry; see Figure 3. Moreover, in addition to having different threshold velocities, the collisions along various directions proceed along different reaction pathways, as will be discussed below.

Collisions normal to the (001), (110), and (011) planes can be considered more sensitive because their threshold velocities are lower. The (111) collision case produced reactions at the intermediate threshold velocity of 4.2 km/s. Finally, collisions normal to the (010), (100), and (101) planes are more insensitive with threshold velocities well above 4.0 km/s which is considered to be a typical particle velocity behind the shock wavefront.[67] In the study performed by Wu et al.,[61] comparable threshold velocities were found for the (001), (100), and (110) head-on collision cases, though glancing collisions showed much lower threshold velocities than those found in our study. This is not unexpected because the glancing collisions studied by Wu et al.[61] involved molecules that were initially deformed to impose external conditions corresponding to the maximum resolved shear stresses on slip systems of PETN.[67] As is seen in Figure 3, there is no special preference in chemical reactivity for either glancing or head-on collisions under ambient conditions.

Given the relatively large velocities of the colliding molecules, one might ask whether such collisions would result in appreciable electronic excitations. In principle, such a question can be answered if both the ground and excited state potential energy surfaces (PES) are known. However, there is some indirect evidence that such excitations during hypervelocity collisions with velocities of ~1−10 km/s might not be important. In particular, our classical trajectory simulations deal with the chemical reactions that evolve on a single potential energy surface of the electronic ground state of the system—the adiabatic approximation. The Born−Oppenheimer approximation assumes that, during the collisions, the electronic state of the system evolves from reactants to products at a time scale which is fast compared to the nuclear motion. Qualitatively, nonadiabatic excitation transitions could occur if the velocities of the individual atoms are of the order of electron velocities in the atoms, i.e., 10^8 cm/s = 1000 km/s. More quantitatively, the efficiency of the nonadiabatic transitions is assessed by calculating the Massey parameter: if $a\Delta E/\hbar v \leq 1$, then the nonadiabatic processes, including electronic excitations, have an appreciable probability. Here, $a \sim 5$ Å is the length of the interaction region, ΔE is the ground and excited PES separation, and $v \sim 10$ km/s is the velocity of the molecular collision. Assuming that $\Delta E \sim 1$ eV, the Massey parameter would be ~100. Therefore, for appreciable electronic excitations to take place, the energy separation should be $\Delta E \sim 0.01$ eV. Although in the present work we cannot calculate the excited state PES using ordinary DFT, there are some indications that both the ground and excited states are well-separated. In particular, our DFT calculations of the PETN molecular crystal under both uniaxial and hydrostatic compressions show that the band gap is several eV at pressures up to 100 GPa.[73] Taking into account that DFT systematically underestimates the band gaps, the real separation of ground and excited PES is expected to be even larger.

III. Threshold Velocities to Initiate Chemical Reactions

We found a correlation between experimentally observed shock sensitivities reported by Dick and Yoo et al.[56,67] and the threshold velocities for initiating chemistry; see Table 1. Essentially, the initiation pressures shown in the right column of Table 1 are a measure of the sensitivity for a given direction in bulk PETN. Known sensitive cases with lower initiation pressures have lower threshold velocities than the known insensitive cases with higher initiation pressures.

For example, two compression directions, normal to (001) and (110), were observed to be the most sensitive directions with initiation pressures of 12.1 and 4.2 GPa, respectively. And the threshold velocities 3.30 and 3.9 km/s for head-on (001) and (110) collisions are indeed among the lowest of all collision cases studied (no experimental data was available for shock compression normal to (011) which actually shows the greatest sensitivity for collisions). In contrast, the (100) case proved to have a high threshold velocity of 4.7 km/s which correlates with the high initiation pressure of 22.8 GPa determined by Yoo.[56] The (101) case also has high threshold velocities for all three glancing collisions—6.6, 4.6, and 4.4 km/s—which correlates with experiment in that initiation was not observed upon the application of shock normal to (101) for pressures less than the PETN Chapman−Jouguet pressure of 31 GPa. It is important to note that the correlation between detonation pressure and threshold velocity is merely suggestive, especially when comparing the pressures and velocities for the sensitive cases which include the so-called anomalous shock response of the (110) case (discussed below).[67]

The number of products formed in reactive threshold cases shown in Table 1 can also serve as an indicator of the directional dependence of chemical initiation; see Figure 4. While one might expect more products to form with higher collision velocities, we observed some deviations from this trend. This is evident when comparing (010) mol. 1−2, (010) mol. 1−4, and (011) mol. 1−2, having threshold velocities of 4.7, 4.4, and 5.3 km/s, respectively, with (100), (101) mol. 1−2, and (101) mol. 1−3, having threshold velocities of 4.7, 6.6, and 4.6 km/s. The collisions in the first group all produce only one fragment, while the collisions of the second group all produce three fragments. In short, the number of products produced by a collision depends as much on the orientation as it does on the collision energy. Probing the issue of product formation deeper, one can look at the number of products formed for all collision velocities of any particular direction and see once again that product number does not necessarily scale with collision energy; see Figure 4.

Though the number of products increases with collision velocity in cases like (111) head-on and (110) glancing, other cases such as (100) head-on and (101) mol. 1−7 glancing show that the number of products can diminish at higher collision velocities. One interesting example of this is the (001) head-on case in which a single product is produced at 3.3 km/s, and no products are produced at 3.4 km/s. The reason for this is hidden

TABLE 1: Threshold Velocities, Products, Times of Product Formation, and Experimentally Determined Initiation Pressures for Bulk PETN[a]

hkl	type	mol.	vel (km/s)	N prod.	species	Rx time (fs)	exp. press. (GPa)
001	head-on	1−3	3.30	1	NO_2	450	12.1
010	glancing	1−2	4.70	1	NO_2	135	
							N/A
	head-on	1−4	4.40	1	NO_2	410	
011	glancing	1−2	5.30	1	NO_2	110	
							N/A
		1−3	3.40	1	NO_2	130	
		1−5	3.20	1	NO_2	225	
100	head-on	1−6	4.70	3	NO_2, H_2CO, NO_2	130,160, 420	
							22.8
101	glancing	1−2	6.60	4	NO_2, NO_2, H_2CO, NO_2	90, 245,316,480	
							no Rx[b]
		1−3	4.60	3	NO_2, NO_2, H_2CO	90, 135, 160	
							$P < 31$
		1−7	4.40	2	NO_2, NO_2	155, 415	
110	glancing	1−2	4.50	1	NO_2	160	
							4.2
	head-on	1−8	3.90	2	HONO, CO	310, 310	
111	head-on	1−2	4.20	2	NO_2, NO_2	140, 295	
							N/A

[a] The molecular indices in column 3 match those labeling each molecule in Figure 1. [b] PETN is believed to detonate at or above the Chapman−Jouguet pressure of 31 GPa for the (101) direction.

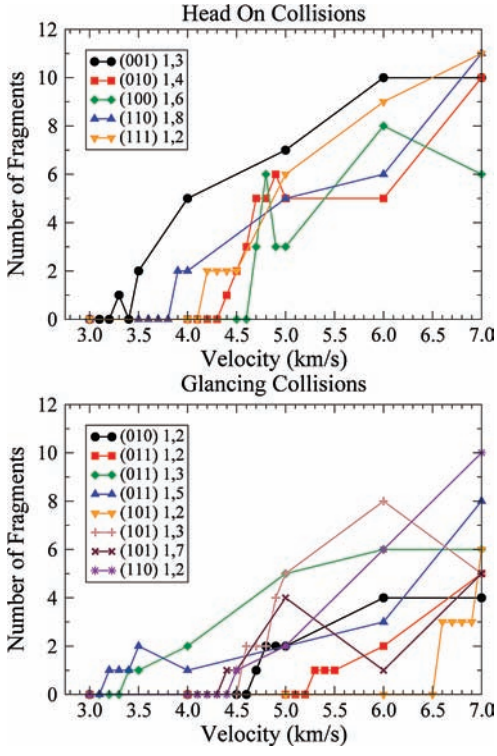

Figure 4. Number of fragments produced vs collision velocity for head-on collisions (top) and glancing collisions (bottom).

in the details of the dynamics of the simulations. In the 3.3 km/s case, which is discussed later in Figure 6, the reacting nitro group is imparted with translational kinetic energy as the connecting arm is thrown outward. As the associated O−NO_2 bond stretches in its oscillation, the connecting formaldehyde group snaps back toward its original configuration, leaving the NO_2 behind. In the 3.4 km/s case, the formaldehyde does not snap back quite as fast due to a twisting deformation in the center of the molecule. As a result, the O−NO_2 bond that was severed in the 3.3 km/s case is not severed in the 3.4 km/s case. While this result may be due to the thermal fluctuations, the amplitudes of the O−NO_2, C−C, and C−O thermal vibrations are small (∼0.1 Å), making it unclear whether or not thermal effects are at play.

IV. Reaction Pathways

Several studies have addressed a correlation between bond dissociation energies (BDEs) and impact sensitivities of various colliding compounds.[61,74−76] Wu et al. conducted such a study[61] for PETN by calculating BDEs for PETN using DFT with the BPW91 GGA functional. They found that the dominant reaction pathway was the dissociation of the O−NO_2 single bond leading to the formation of NO_2. They found that the O−NO_2 single bond was indeed the weakest bond in PETN with a BDE of 157.8 kJ/mol.[61] Another study[74] by Fried et al. also found the single O−NO_2 bond to be weakest with a BDE of 167 kJ/mol. We performed our own study of the BDEs for PETN including all bonds within the PETN molecular complex. Figure 5 shows these BDEs for the intact molecule, as well as the BDE of the C−C bond after the dissociation of the connecting NO_2.

In agreement with the study of Wu et al., we found NO_2 production to be the dominant chemical event in our simulations. Every reactive collision performed in this study began with the disassociation of the O−NO_2 bond leading to an NO_2 product, as seen in Table 1. This commonality can be at least partly attributed to the relative weakness of the O−NO_2 bond (182.69 kJ/mol) in the nonreacted PETN molecular complex, as seen in Figure 5. It is clear from the BDEs why we do not see the dissociation of other bonds within the molecule first. It should be pointed out that some studies[28,77] have suggested that the O−NO_2 bond is not the first to break when PETN is exposed to high energy laser radiation, or high pressure; rather, they suggest that the C−C and C−O bonds are the first to break. In

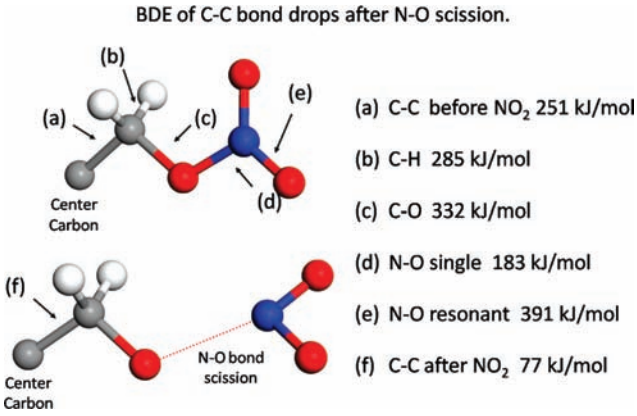

Figure 5. Bond dissociation energies for PETN in kJ/mol calculated using the PBE functional.

the work[77] by Zhurova et al., which cites the high electron density value of the O−NO_2 bond, we assert that it is the bond order, not the electron density, which determines the breaking of the bond. Also, in reference to the work[28] by Ng et al., which finds no peak for NO_2 in a mass spectrometry study of laser decomposed PETN, we point out that the time resolution required to see the initial stages of chemical initiation is ∼1 ps, not ∼100 μs.

The next weakest bond in the PETN complex is the C−C bond with a BDE of 250.48 kJ/mol. This particular bond scission occurred less frequently in threshold cases but was nonetheless prevalent, occurring only after or during the dissociation of the O−NO_2 bond in the reacting arm. We calculated the BDE for the C−C bond after the dissociation of the accompanying O−NO_2 bond and found a drop in energy from 250.48 kJ/mol to only 77.07 kJ/mol. The lowering of the BDE for the C−C bond may explain why H_2CO forms instead of more NO_2 fragments; such a reaction pathway is actually favored by the low value of BDE. From Table 1, it is evident that some threshold cases produced multiple NO_2 fragments without producing H_2CO. In both such cases for glancing collisions in the (101) direction, only the outer nitro groups of the colliding PETN molecules interacted, leaving the interiors relatively intact. Likewise, the (111) head-on threshold collision was oriented such that the nitro groups in multiple arms took the brunt of the collision simultaneously, allowing no close approach to the interior of either molecule. In other collisions in which multiple fragment types were formed, close approaches affecting the interiors of the reacting molecule were prevalent. It therefore must be concluded that, while BDEs can account for part of the chemical phenomena seen in our simulations, the actual dynamics of the collisions must also be considered for a more complete picture of the initiation of chemistry to emerge.

V. Reaction Dynamics

Apart from the BDEs of the various bonds in the PETN molecular complex, a study of the dynamic factors of collisions is necessary to understand the localized transfer of energy leading to the rapid reactions seen in our simulations. As a starting point, we looked at the simple dissociation of the O−NO_2 bond in single product threshold cases such as the (001) head-on collision. The depiction in Figure 6 shows various important stages leading to the formation of NO_2 for the (001) collision.[70] Upon collision, the approaching arms in the left molecule are thrown outward; see Figure 6b and c. The nitro group at the top of the left molecule continues to move to the left as the connecting formaldehyde group recoils back to the right (Figure 6d and e). Because of this opposing motion, the O−NO_2 bond connecting the nitro group to the formaldehyde group is stretched to the breaking point (Figure 6f). Essentially, the entire arm was moved out of its equilibrium position, and like a loaded spring tended to return to its original state. However, while the inner part (the formaldehyde group) recoiled back toward its equilibrium position, the nitro group was prevented from doing so by its momentum. Figure 6g shows a plot of the bond lengths for the O−NO_2, C−C, and C−O bonds within the reacting arm. The C−C and C−O bonds remain out of phase during the stretching periods of the O−NO_2 bond—the carbon atom within the arm is moving between the connecting oxygen and center carbon. When the C−C and C−O bonds finally come into phase, the oxygen atom is pushed to the right as both bonds stretch, severing the O−NO_2 bond. Then, the carbon atom is pulled back down as both the C−C and C−O bonds contract, making the O−NO_2 scission permanent.

In general, the loading of the bonds in the reacting molecule is mainly localized to only those parts immediately affected by the collision. A prime example of this is the (100) head-on threshold case, shown in Figure 7, in which an O−NO_2 bond is immediately broken as a nitro group from the right molecule strikes the reacting nitro group in the left molecule almost laterally.[71] The O−NO_2 bond scission is immediately followed by a C−C bond scission and subsequently by another O−NO_2 bond.

The O−NO_2 bond scission happens fast, occurring before any massive deformation to the rest of the reacting molecule (Figure 7a−c). The stretching mode of the O−NO_2 bond in the nonreacting molecule on the right is loaded as it pushes against the first reacting nitro group on the left. As seen in Figure 7g, the amplitude of the O−NO_2 stretching mode in the nonreacting molecule increases once the O−NO_2 bond in the reacting molecule is cleaved. With the majority of the collision energy localized in the reacting arm, the connecting formaldehyde group is pulled down, stretching the associated C−C bond to its breaking point (Figure 7d). As discussed earlier, the BDE for the O−NO_2 bond is initially the lowest (182.69 kJ/mol) in the molecular complex; however, once the O−NO_2 bond breaks, the BDE for the associated C−C bond drops significantly to become the lowest (from 250.48 kJ/mol down to 77.07 kJ/mol) which can in part account for the reaction pathway seen here. In Figure 7e, the upper arm of the reacting molecule begins a downward swing, bending sharply between the central carbon atom and the formaldehyde group. The bend is so sharp that the oxygen atom in the formaldehyde group bonds with the central carbon atom while the downward motion of the nitro group and the stretching of the associated O−NO_2 bond leads to the formation of another NO_2 (Figure 7f). The fact that this reaction pathway occurred as described offers supporting evidence that the chemical initiation due to a hypervelocity collision is not thermal. If the reactions were thermal, then the formation of NO_2 and H_2CO would not have been immediate. At the very least, they would have had to occur only after some number of oscillations of their associated modes of vibration. It is also important to note that between frames d and f in Figure 7, some of the nitro groups in the nonreacting molecule seemed to dissociate temporarily, as seen in Figure 7f. If these apparent dissociations, which were identified by extremely large bond lengths, can indeed be considered reactions, then these nitro groups reform as they travel along trajectories similar to their parent molecule.

The rarest reaction pathway observed in the threshold collision cases involves C−H bond scissions at a rather low collision

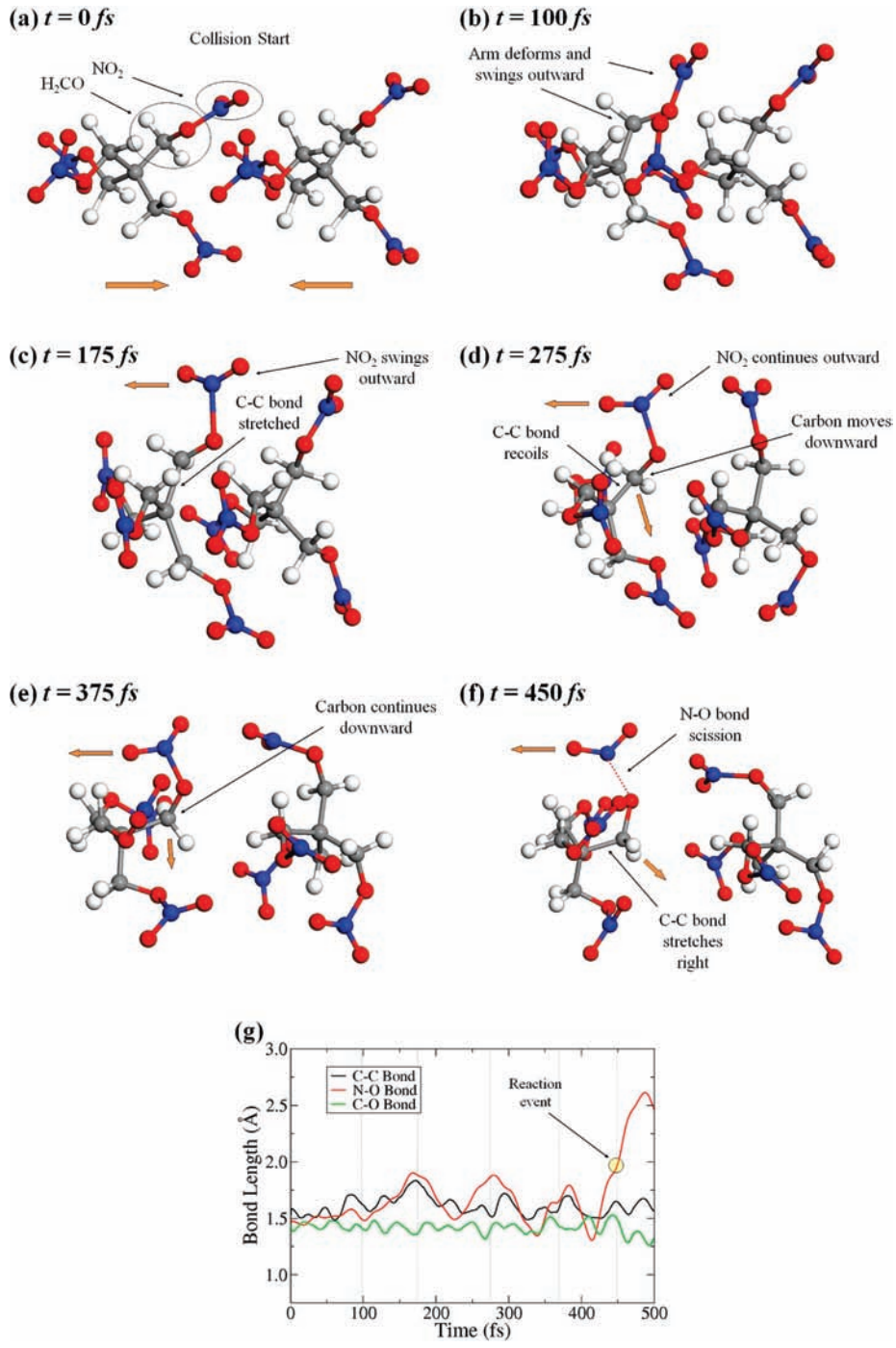

Figure 6. Case of (001), head-on, mol. 1−3, 3.3 km/s collision: (a−f) collision dynamics leading to an O−NO_2 bond scission; (g) bond lengths plotted against tine. The vertical lines show the frames depicted in parts a−f.

velocity. In the (110) head-on threshold case, NO_2 is formed in much the same manner as in the (001) threshold case. H_2CO forms almost immediately after the formation of NO_2 in a manner similar to that of the (100) threshold case. These products form almost simultaneously and have rotations imparted to them. As a result, the hydrogen atoms in the H_2CO come within bonding distance of both the central carbon atom of the reacting molecule, and an oxygen atom in the NO_2 causing the C−H bond scissions, as depicted in Figure 8a−d.[72]

The C−H reaction events can be seen in Figure 8e where the plots of the bond lengths of the reactants cross those of the resulting products. The thermal behavior of the hydrogen bonds is evident before and after the reaction events. It is interesting to point out that a study[67] done by Dick, which reported an anomalous shock response normal to (110) at 4.2 GPa, also reported Raman spectra data that suggested the formation and decomposition of HONO. Another interesting study[39] by Wu et al. suggested the importance of HONO as an intermediate in water catalysis which was shown to speed up the thermal decomposition of EMs. It is possible that the early formation of HONO at such a low threshold velocity as seen in our collision simulation of (110) may be responsible for the anomalous shock response[67] observed by Dick, especially since the (110) head-on collisions were the only set of collisions that produced HONO with collision velocities below 5 km/s, with the (111) head-on collisions being the only other set to produce

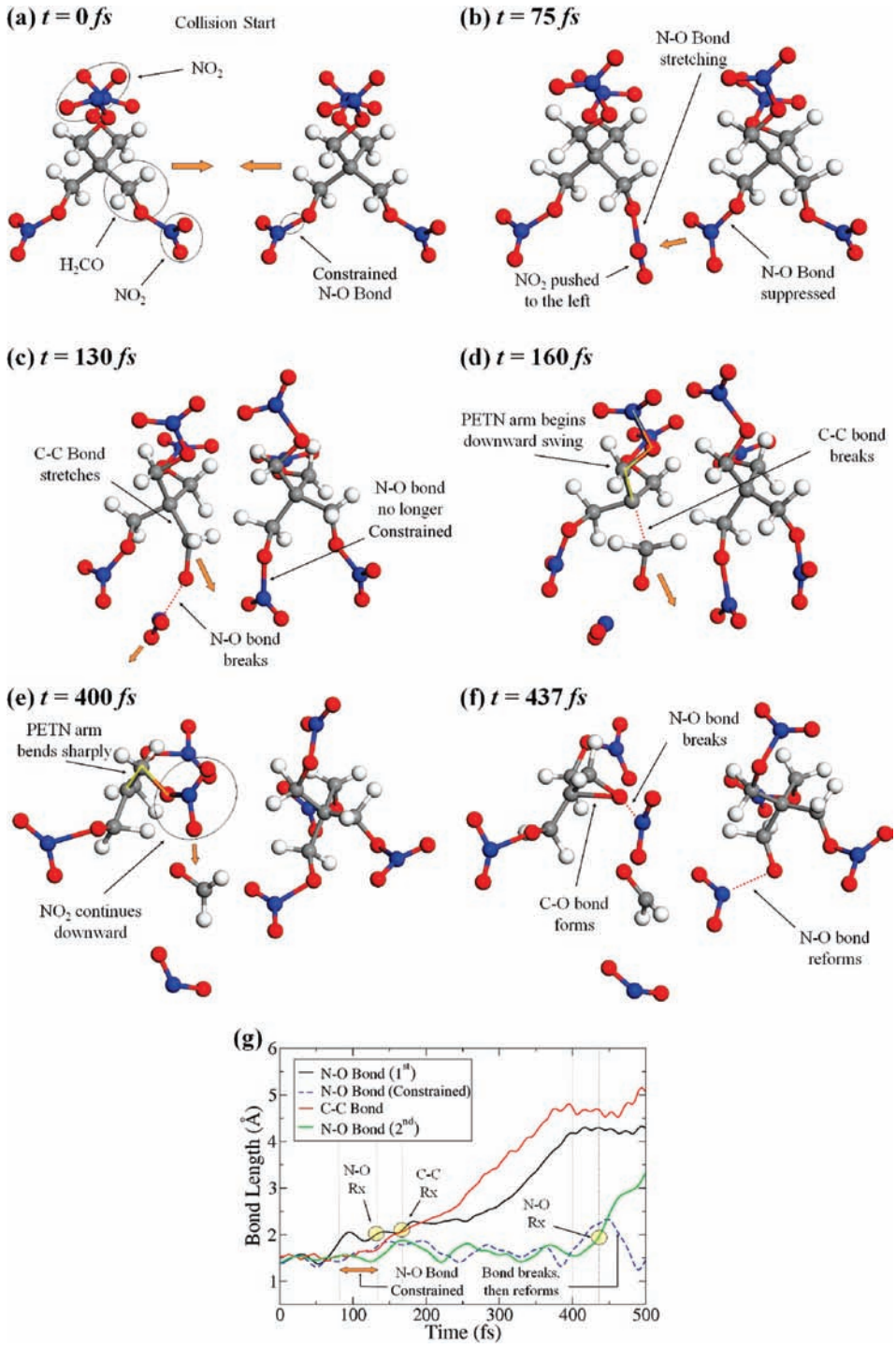

Figure 7. Case of (100), head-on, mol. 1−6, 4.7 km/s collision: (a−f) collision dynamics leading to O−NO_2, C−C, and O−NO_2 bond scissions; (g) bond lengths plotted against time. The vertical lines show the frames depicted in parts a−f; the bond length of the constrained, nonreacting N−O bond responsible for the first reaction is represented by a dashed line.

HONO below 6 km/s (though (111) was not included in the experimental studies of Dick et al.). Because C−H thermal vibrations were at play in the formation of CO and HONO, and because of the unique reaction dynamics, we performed another simulation of the (110) head-on collision at the same threshold velocity of 3.9 km/s. In this simulation, we equilibrated the bimolecular complex to 310 K to investigate the possibility that the reaction pathway we observed in the first simulation might have been a statistical aberration. We found that the sequence of chemical events in the 310 K case was nearly identical to that in the 300 K case, differing only in that the events occurred about 15 fs earlier in the later simulation. This suggests that thermal factors leading up to the reaction within a comparable temperature range do not affect the reaction pathway in this case—the formation of HONO and CO is an intrinsic property of the (110) head-on collision case at the threshold velocity. The C−H scissions occurred due to a combination of the relatively slow rotation of the H_2CO, the fast thermal vibrations of the C−H bonds, and the proximity of the H_2CO to the NO_2 and parent molecule. When we looked at similar reactions involving C−H scissions in some of the high energy collisions, we found the reaction mechanism to be

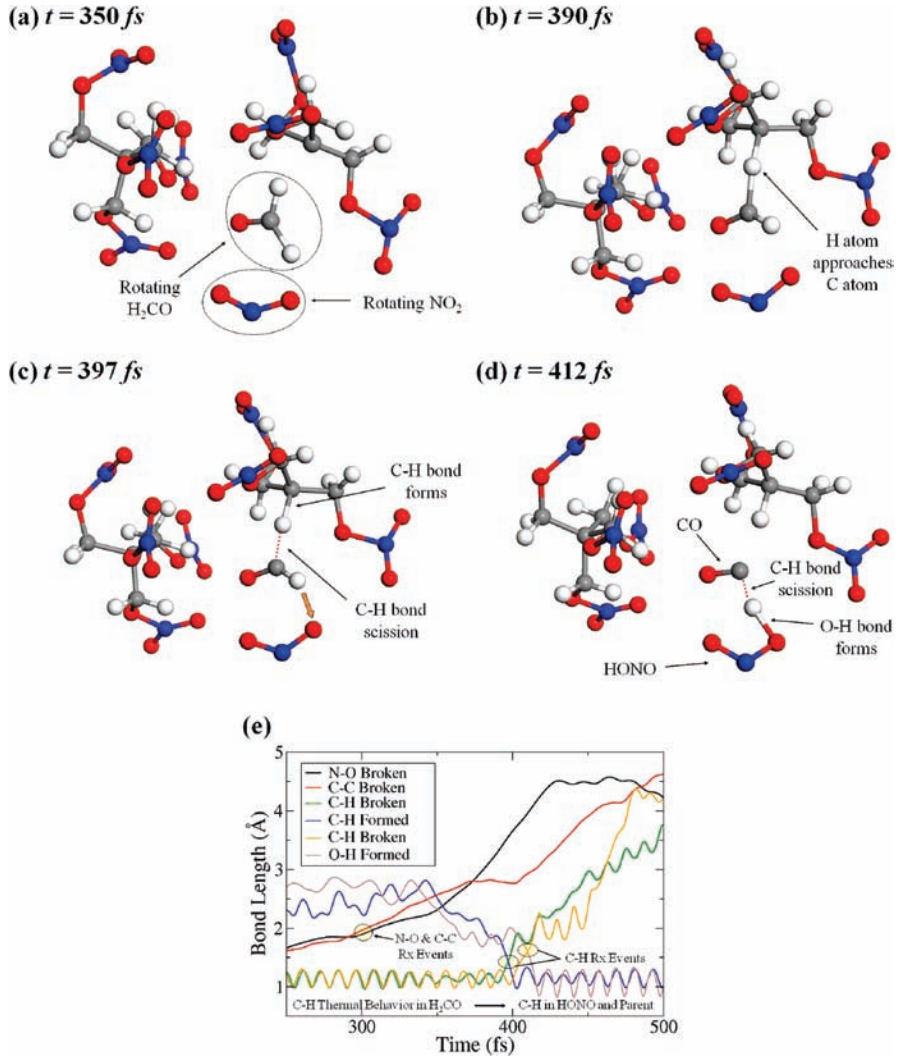

Figure 8. Case of (110), head-on, mol. 1−8, 3.9 km/s collision: (a−d) collision dynamics leading to C−H reaction events; (e) bond lengths of both reactants and products plotted over the entire time of simulation.

roughly the same—either an oxygen atom from a fragment or a central carbon from a reacted PETN molecule passes within bonding distance of a hydrogen atom and steals it away from the connecting carbon in a formaldehyde group.

VI. Nonequilibrium Chemistry

We found from our simulations that the hypervelocity reactions of colliding molecules in PETN are due to a combination of mechanical deformation, steric proximity, and localized vibrations (excited or thermal in the case of hydrogen). Obviously, due to the very short time scale of the reactions (on the order of 100 fs), thermal equilibrium does not exist. Therefore, classical transition state theory (which implies thermal equilibrium within reactant and product subsystems, and between those subsystems and the activated complex[18]) does not apply to the case of hypervelocity collision reactions, which we assume to be the cause of initiation of chemical reaction behind a detonation front. In Table 1, we see that reactions occur between 100 and 500 fs which puts the reaction time scale at $\sim 10^{-13}$ s, exactly what was suggested by Walker et al.[54,55] If one were to assume that there is such thermal equilibrium, then there are problems that must be confronted. For instance, assuming that the entire kinetic energy of the translational degrees of freedom within the colliding PETN molecules for a 4 km/s collision is distributed throughout all of the internal degrees of freedom within the binary collision complex, the system would have a temperature of 2000 K. This thermal equilibration should take place during tens of picoseconds ($\sim 10^{-11}$ s).[13] Then, according to TST, the reaction rate of the O−NO_2 bond scission which produces the NO_2 products can be estimated as

$$k_r = f \exp\left(\frac{-E_b}{k_B T}\right) \tag{2}$$

where the N−O stretching mode frequency is $f \sim 10^{13}$ s^{-1} and the O−NO_2 bond dissociation energy is $E_b = 183$ kJ·mol^{-1}. The rate of reaction would then be $k_r \sim 10^8$ s^{-1}, or one reaction every $t = 10$ ns which is 3 orders of magnitude larger than the time required to establish thermal equilibrium ($\sim 10^{-11}$ s). This seems much too slow for the chemical events sustaining a detonation. For example, if we assume a reactive zone of thickness 1 μm behind a shock front traveling with detonation speed $v_s = 7$ km/s, then the time of the passage of the reactive zone would be $t \approx 0.1$ ns. Thus, little, if any, reaction would occur between the von Neumann spike and the C−J point of the detonation wave. In addition, this TST reaction time scale

is several orders of magnitude larger than those seen in simulation. Finally, the orientation dependence of these collisions strongly suggests that thermal processes are not all that is at work here. If the reactions were temperature driven, then energy would be evenly distributed throughout the colliding molecules; thus, any difference in threshold velocities for all possible collision orientations would be statistical in nature. However, the correlation between threshold velocities and detonation pressures suggests that the orientation dependence is real and not a statistical aberration. From this, it must be concluded that these initial chemical events are not temperature driven. Rather, they are driven directly by the dynamics of the collisions and exhibit explicit orientation dependence in a hypervelocity chemical regime.

VII. Conclusions

First-principles reactive molecular dynamics simulations of hypervelocity bimolecular PETN collisions revealed that the threshold velocities for initiating chemistry along directions corresponding to the compression of specific crystallographic planes correlate to the experimental anisotropic sensitivities determined for bulk crystalline PETN.[56,59] Collisions in the (001), (011), and (110) directions are most sensitive with lowest threshold velocities of 3.3, 3.2, and 3.9 km/s, respectively, while collisions normal to the (010), (101), and (100) planes are most insensitive with threshold velocities of 4.4, 4.4, and 4.7 km/s, respectively. The (111) collision case is at the middle of the spectrum with an intermediate threshold velocity of 4.2 km/s. The reactive case simulations show the formation of NO_2 as the dominant reaction pathway in all cases, with H_2CO formation for cases in which a large amount of collision energy is localized in a particular arm of the molecule. In such cases where H_2CO is formed, we find that the bond dissociation energy for the C−C bond drops after the connecting NO_2 group dissociates. An exception was found for the sensitive (110) mol. 1−8 threshold case in which HONO and CO were ultimately produced as a result of atomic proximity and C−H thermal vibrations. A relationship between the steric orientation of the colliding molecules and chemical enhancement is evidenced by both threshold velocities for initiating chemistry and product formation. Reactive cases yielded product formation on time scales of the same order of magnitude as the oscillation periods of the various modes of vibration within the PETN molecule, 10^{-13} s. These reaction time scales are much too short for thermal processes to drive the reactions, leading us to conclude that the direct physical dynamics of the collisions is paramount in sustaining and perhaps initiating a detonation. More specifically, reactions are driven by dynamics that involve mechanical deformation, steric proximity, thermal vibrations (in the case of C−H scission), and localized excitations in vibration modes rather than temperature.

Acknowledgment. The work performed at the University of South Florida was supported by the Office of Naval Research (ONR) through the Naval Research Laboratory (NRL) and partly by the Army Research Office through the Multi-University Research Initiative on Insensitive Munitions. The work at NRL was supported by ONR both directly and through NRL. Calculations were performed using NSF TeraGrid facilities (Grants TG-DRM070018N and TG-MCA08X040), USF Research Computing Cluster, and computational facilities of Materials Simulation Laboratory at the University of South Florida funded by ARO DURIP (Grant No. W911NF-07-1-0212). Visualizations and video rendering were done using Jmol (http://jmol.sourceforge.net/) and RasMol (http://www.rasmol.org/) molecular visualization software. I.I.O. and A.C.L. thank Prof. M. A. Kozhushner for discussions of nonequilibrium chemistry.

References and Notes

(1) Davis, W. C. *Sci. Am.* **1987**, *256*, 106.
(2) *Energetic Materials: Part 1, Decomposition, Crystal and Molecular Properties,* Politzer, P. A., Murray, J. S., Eds.; Elsevier: Amsterdam, 2003; Vol. 12, in the series *Theoretical and Computational Chemistry*, p 45.
(3) *Energetic Materials: Part 2, Detonation, Combustion*; Politzer, P. A., Murray, J. S., Eds.; Elsevier Science: 2003; Vol. 13 in the series *Theoretical and Computational Chemistry*.
(4) *Overview's of Recent Research on Energetic Materials*; Shaw, R. W., Brill, T. B., Thompson, D. L., Eds.; World Scientific Publishing: London, 2005.
(5) Fickett, W.; Davis, W. C. *Detonation: Theory and Experiment*; Dover Publications: Mineola, NY, 2001.
(6) Zeldovich, Ya. B.; Kompaneets, A. S. *Theory of Detonation*; Academic Press: New York, 1960.
(7) Landau, L. D.; Lifshitz, E. M. *Fluid Mechanics*; Butterworth-Heinemann: Oxford, 1987.
(8) Chapman, D. L. *Philos. Mag.* **1899**, *47*, 90.
(9) Jouguet, *J. Math. Pures Appl.* **1906**, *1*, 347.
(10) Ya, B. *Zh. Eksp. Teor. Fiz.* **1960**, *10*, 542.
(11) Doering, W. *Ann. Phys.* **1943**, *43*, 421.
(12) von Neumann, J. Office of Science Research and Development: Report No. 549 (1942).
(13) *Energetic Materials: Part 1, Decomposition, Crystal and Molecular Properties,*; Politzer, P. A., Murray, J. S., Eds.; Elsevier Science: 2003; Vol. 12 of the series *Theoretical and Computation Chemistry*, Part 1, p 125.
(14) Melius, C. F. *Phil. Trans. R. Soc. Lond. A: Math., Phys., and Eng Sci.* **1992**, *339* (1654), 365.
(15) Chakraborty, D.; Hsu, C.-C.; Lin, M. C. *J. Chem. Phys.* **1998**, *109*, 8887.
(16) Zhang, S.; Truong, T. N. *J. Phys. Chem. A* **2000**, *104* (31), 7304.
(17) Chakraborty, D.; Muller, R. P.; Dasgupta, S.; Goddard, W. A., III. *J. Comput.-Aided Mater. Des.* **2001**, *8*, 203.
(18) Eyring, H. *J. Chem. Phys.* **1935**, *3*, 107.
(19) Eyring, H. *Science* **1978**, *199* (4330), 740.
(20) Zerilli, F. J.; Toton, E. T. *Phys. Rev. B* **1984**, *29* (10), 5891.
(21) Dlott, D. D.; Fayer, M. D. *J. Chem. Phys.* **1990**, *92*, 3798.
(22) Tokmakoff, A.; Fayer, M. D.; Dlott, D. D. *J. Phys. Chem.* **1993**, *97*, 1901.
(23) Fried, L. E.; Ruggiero, A. J. *J. Phys. Chem.* **1994**, *98*, 9786.
(24) Ye, S.; Koshi, M. *J. Phys. Chem. B* **2006**, *110*, 18515.
(25) Tarver, C. M.; Forbes, J. W.; Urtiew, P. A. *Russ. J. Phys. Chem. B* **2007**, *1*, 39.
(26) Oxley, J. C. *Energetic Materials: Part 1, Decomposition, Crystal and Molecular Properties*; Politzer, P. A., Murray, J. S., Eds.; Elsevier Science: 2003; Vol. 12 of the series *Theoretical and Computational Chemistry*, p 5.
(27) Ng, W. L.; Field, J. E.; Hauser, H. M. *J. Chem. Soc., Perkin Trans.* **1976**, *6*, 637.
(28) Ng, W. L.; Field, J. E.; Hauser, H. M. *J. Appl. Phys.* **1986**, *59*, 3945.
(29) Tarver, C. M.; Tran, T. D.; Whipple, R. E. *Propellants, Explos., Pyrotech.* **2003**, *28*, 189.
(30) Dreger, Z. A.; Gruzdkov, Yu. A.; Gupta, Y. M.; Dick, J. J. *J. Phys. Chem. B* **2002**, *106*, 247.
(31) Robertson, D. H.; Brenner, D. W.; White, C. T. *Phys. Rev. Lett.* **1991**, *67*, 3132.
(32) Chakraborty, D.; Muller, R. P.; Dasgupta, S.; Goddard, W. A., III, *J. Phys. Chem. A* **2000**, *104*, 2261.
(33) Lewis, J. P.; Glaesemann, K. R.; VanOpdorp, K.; Voth, G. A. *J. Phys. Chem. A* **2000**, *104*, 11384.
(34) Rice, B. M.; Thompson, D. L. *J. Chem. Phys.* **1990**, *93*, 7986.
(35) Sewell, T. D.; Thompson, D. L. *J. Phys. Chem.* **1991**, *95*, 6228–6242.
(36) Manaa, M. R.; Fried, L. E.; Melius, C. G.; Elsner, M.; Frauenheim, T. *J. Phys. Chem. A* **2002**, *106*, 9024.
(37) Manaa, M. R.; Fried, L. E.; Galli, G.; Gygi, F. *J. Chem. Phys.* **2004**, *120*, 10146.
(38) Reed, E. J.; Manaa, M. R.; Fried, L. E.; Glaesemann, K. R.; Joannopolous, J. D. *Nat. Phys.* **2008**, *4*, 72.
(39) Wu, C. J.; Fried, L. E.; Yang, L. H.; Goldman, N.; Bastea, S. *Nat. Chem.* **2009**, *1*, 57.
(40) Kuklja, M. M.; Kunz, A. B. *J. Appl. Phys.* **2001**, *87*, 2215.
(41) Kuklja, M. M.; Kunz, A. B. *J. Appl. Phys.* **2001**, *89*, 4962.

(42) Kuklja, M. M.; Aduev, B. P.; Aluker, E. D.; Krasheninin, V. I.; Krechetov, A. G.; Yu, A. *J. Appl. Phys.* **2001**, *89*, 4156.
(43) Elert, M. L.; Deaven, D. M.; Brenner, D. W.; White, C. T. *Phys. Rev. B* **1989**, *39*, 1453.
(44) White, C. T.; Robertson, D. H.; Elert, M. L.; Brenner, D. W. Molecular Dynamics Simulations of Shock-Induced Chemistry: Application to Chemically-Sustained Shock Waves. In *Microscopic Simulations of Complex Hydrodynamic Phenomena*; Mareschal, M., Holian, B. L., Eds.; Nato Science Series B; Plenum Press: New York, 1992; p 111.
(45) Brenner, D. W.; Robertson, D. H.; Elert, M. L.; White, C. T. *Phys. Rev. Lett.* **1993**, *70*, 2174.
(46) White, B. L.; Swanson, D. R.; Robertson, D. H. Molecular Dynamics Simulations of Detonations. In *Chemical Dynamics in Extreme Environments*; Dressler, R. A., Ed.; World Scientific Publishing: Princeton, NJ, 2001.
(47) Mintmire, J. W.; Robertson, D. H.; White, C. T. *Phys. Rev. B* **1994**, *49*, 14859.
(48) van Duin, A. C. T.; Dasgupta, S.; Lorant, F.; Goddard, W. A., III, *J. Phys. Chem. A* **2001**, *105*, 9396.
(49) Strachan, A.; van Duin, A. C. T.; Chakraborty, D.; Dasgupta, S.; Goddard, W. A., III, *Phys. Rev. Lett.* **2003**, *91*, 098301.
(50) Strachan, A.; Kober, E. M.; van Duin, A. C. T.; Oxgaard, J.; Goddard, W. A., III, *J. Chem. Phys.* **2005**, *122*, 054502.
(51) Nomura, K. I.; Kalia, R. K.; Nakano, A.; Vashishta, P.; van Duin, A. C. T.; Goddard, W. A., III, *Phys. Rev. Lett.* **2007**, *99*, 148303.
(52) Budzien, J.; Thompson, A. P.; Zybin, S. V. *J. Phys. Chem B* **2009**, *113*, 13142.
(53) Dremin, A. N. *Philos. Trans. R. Soc. London, Ser. A* **1992**, *339*, 355.
(54) Walker, F. E. *J. Appl. Phys.* **1988**, *63*, 5548.
(55) Walker, F. E. *Propellants, Explos., Pyrotech.* **1994**, *19*, 315.
(56) Yoo, C. S.; Holmes, N. C.; Sours, P. C.; Wu, C. J.; Ree, F. H. *J. Appl. Phys.* **2000**, *88* (1), 70.
(57) Dick, J. J. *J. Appl. Phys.* **1997**, *81*, 601.
(58) Dick, J. J.; Ritchie, J. P. *J. Appl. Phys.* **1994**, *76*, 2726.
(59) Dick, J. J. *Appl. Phys. Lett.* **1984**, *44*, 859.
(60) Selezenev, A. A.; Yu, A.; Briginas, I. V. *Russ. J. Phys. Chem. B* **2008**, *2*, 147.
(61) Wu, C. J.; Ree, F. H.; Yoo, C. S. *Propellants, Explos., Pyrotech.* **2004**, *29* (5), 296.
(62) Wei, D.; Zhang, F.; Woo, T. K. Proceedings of the 12th Biennial International Conference of the APS Topical Group on Shock Compression of Condensed Matter (2001).
(63) Decker, S. A.; Woo, T. K.; Wei, D.; Zhang, F. *Chem. Phys. Lett.* **2003**, *373*, 498.
(64) Stewart, J. J. P. *J. Comput. Chem.* **1989**, *10*, 209.
(65) Stewart, J. J. P. *J. Comput. Chem.* **1989**, *10*, 221.
(66) Besler, B. H.; Hase, W. L.; Hass, K. C. *J. Phys. Chem.* **1992**, *96*, 9369.
(67) Dick, J. J.; Mulford, R. N.; Spencer, W. J.; Pettit, D. R.; Garcia, E.; Shaw, D. C. *J. Appl. Phys.* **1991**, *70* (7), 3572.
(68) Spanish Initiative for Thousands of Atoms, http://www.icmab.es/siesta/.
(69) Perdew, J. P.; Burke, K.; Ernzerhof, M. *Phys. Rev. Lett.* **1996**, *77* (18), 3865.
(70) http://msl.cas.usf.edu/PETN_Col/PETN_001.mpg.
(71) http://msl.cas.usf.edu/PETN_Col/PETN_100.mpg.
(72) http://msl.cas.usf.edu/PETN_Col/PETN_110.mpg.
(73) Conroy, M.; Oleynik, I. I.; Zybin, S. V.; White, C. T. *Phys. Rev. B* **2008**, *77*, 094107.
(74) Fried, L. E.; Manaa, M. R.; Pagoria, P. F.; Simpson, R. L. *Annu. Rev. Mater. Res.,* **2001**, *31*, 291.
(75) Cao, C.; Gao, S. *J. Phys. Chem. B* **2007**, *111*, 12399.
(76) Fang, M.; Zhe, L.; Fu, Y. *Chin. J. Chem.* **2008**, *26*, 1122.
(77) Zhurova, E. A.; Stash, A. I.; Tsirelson, V. G.; Zhurov, V. V.; Bartashevich, E. V.; Potemkin, V. A.; Pinkerton, A. A. *J. Am. Chem. Soc.* **2006**, *128* (45), 14728.

JP905969Y